Optics Letters

Electronic states of defect with impurity and infrared emission on black silicon prepared by an ns-laser

Zhong-Mei Huang,[1,2] Wei-Qi Huang,[1,*] Zui-Min Jiang,[2] Shi-Rong Liu,[3] Xue-Ke Wu,[1] and Chao-Jian Qin[3]

[1]Institute of Nanophotonic Physics, Guizhou University, Guiyang 550025, China
[2]State Key Laboratory of Surface Physics, Key Laboratory of Micro and Nano Photonic Structures (Ministry of Education) and Department of Physics, Fudan University, Shanghai 200433, China
[3]State Key Laboratory of Environmental Geochemistry Institute of Geochemistry, Chinese Academy of Science Institute of Geochemistry, Guiyang 550003, China
*Corresponding author: wqhuang@gzu.edu.cn

Received 2 November 2016; accepted 9 December 2016; posted 15 December 2016 (Doc. ID 279814); published 12 January 2017

It is found that the optimum annealing temperature is about 1000°C for the infrared emission of defect states at room temperature on black silicon (BS) prepared by using a nanosecond-pulsed laser. In addition, it is observed that the suitable annealing time is $6 \sim 8$ min at 1000°C for the emission on the BS. The crystallizing proceeding in annealing on the BS can be used to explain the above annealing effect. It is interesting that the emission band becomes intensive and broader on the BS prepared in oxygen atmosphere than that prepared in vacuum in the analysis of photoluminescence spectra, where the electronic states localized at the defects from D1 to D4 doped with oxygen play an important role in the emission with the broader band which are obviously enhanced in the room temperature.

OCIS codes: (140.3538) Lasers, pulsed; (160.2220) Defect-center materials; (250.5230) Photoluminescence; (300.6340) Spectroscopy, infrared.

https://doi.org/10.1364/OL.42.000358

Eric Mazur's group obtained micro-structure black silicon (BS) prepared by using a femtosecond (fs) laser whose light absorption exceeds 90% [1–6]. The BS is an amazing material with potential application in the field of Si-based optoelectronic devices, including novel detectors, sensors, and solar cells [7,8]. Recently, the photoluminescence (PL) in the optical-communication window on the BS has attracted scientific interest [9–13]. For optimizing the BS qualities for emission, the annealing is a widely adopted method to improve the photoluminescence efficiency [14,15]. However, the optimal annealing conditions still need to be determined, and the physical mechanism of the annealing process requires further investigation in the complex micro-nano-system. Meanwhile, it is unclear how to affect the infrared emission for the impurity states on the BS.

In the Letter, we report the BS structures fabricated by using a nanosecond laser (ns-laser), in which the efficient emission in infrared emission near 1550 nm was observed. We have found the optimal annealing conditions to improve the emission efficiency on the BS, in which the optimum annealing temperature is about 1000°C, and the suitable annealing time is $6 \sim 8$ min for the infrared emission of the defect states at room temperature on the BS prepared by using ns-laser. This observation implies the potential in fabricating silicon-based solid-state lighting and light sources for optical communication. The crystallizing proceeding in annealing on the BS can be used to explain the above annealing effect. It is interesting that the emission band becomes intensive and broader on the BS prepared in oxygen atmosphere than that prepared in vacuum in the analysis of photoluminescence (PL) spectra, where it is discovered that the impurity states in the bandgap localized at the defects D1, D2, D3 and D4 doped with oxygen generate the broader band emission which are obviously enhanced in the room temperature. This is a new way to make a light source for optical communication on the BS.

An ns-laser is used to fabricate the BS structures in the pulsed laser etching device (PLE), as shown in Fig. 1(a), in which the spot diameter of laser beam is about 1 μm focused on the silicon wafers of a P-type substrate with 10 Ωcm in vacuum (sample I) or in an oxygen environment with 80 Pa (sample II). It is interesting that the plasma lattice pattern occurs in the etching process of the BS, as shown in the inset of Fig. 1(a). Figure 1(b) shows the annealing process on the BS after etching, which is very important for its crystallizing to improve emission properties. The SEM image in Fig. 1(c) shows the micro-structure on the BS prepared by using an ns-laser, where the reflective rate is lower than 10% and the refractive index is about 1.88 in visible range on the SiO_2 surface. The experimental result obeys the K-K relations.

The samples are sent into the annealing furnace filled with Ar atmosphere to make annealing at 600°C, 800°C, 900°C, 1000°C, or 1100°C for 8 min, and take annealing time 2, 6, 8, 10, or 15 min, respectively, as comparison groups.

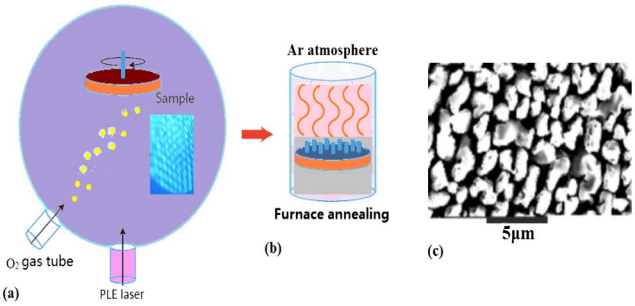

Fig. 1. (a) PLE device used to fabricate the BS structures, in which the inset shows the plasma lattice pattern occurring in the etching process of the BS. (b) Annealing process on the BS after etching for its crystallizing to improve emission properties. (c) SEM image of the BS structure prepared on a p-type silicon (100) wafer by a third harmonic of an ns-pulsed Nd:YAG laser at 355 nm in vacuum.

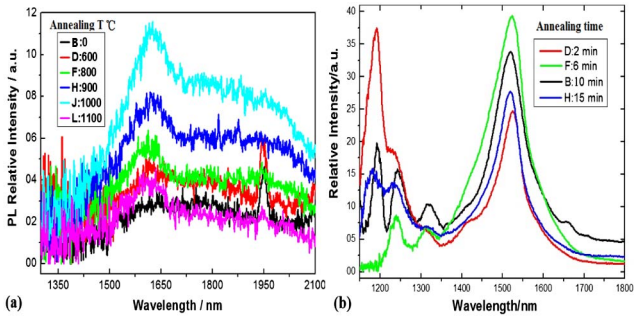

Fig. 3. Analysis of PL spectra in the annealing effect on sample I prepared in vacuum. (a) PL peaks measured at room temperature on the BS after annealing at different temperatures, in which the optimal annealing temperature is about 1000°C. (b) PL peaks measured at 16 K on the BS after annealing for different times, in which the suitable annealing time is about 6 min.

The crystallizing process in the annealing of the BS is very important for PL emission. Figure 2 shows various crystallizing structures in the BS prepared under different annealing conditions, in which the TEM images exhibit the BS structures prepared under annealing at 1000°C for 2, 8, or 20 min, as shown in Figs. 2(a)–2(c), respectively. The samples are sent into the annealing furnace filled with Ar atmosphere to make annealing at 1000°C for 2, 6, 8, or 20 min, in which the different temperatures can be controlled in a temperature cruising system. Then, the sample gotten out of the annealing furnace is rapidly taken into water at room temperature for the BS to be rapidly cooled so that the suitable structures at high temperature can be kept for solidification. The PL spectra show that annealing time of $6 \sim 8$ min is suitable for emission. It is clear that the structure of the BS prepared under annealing at 1000°C for 8 min involves more defects, while the structure of the BS prepared under annealing at 1000°C for 2 min still keeps in amorphous structure produced by the ns-laser, and the crystallizing of the BS prepared under annealing at 1000°C for 20 min is almost finished. This annealing effect generated from crystallizing in the BS is demonstrated in the analysis of the PL spectra followed.

The PL spectra on the samples are measured under the 488 nm or 514 nm excitation of an Ar ion laser at room temperature and lower temperature ($16 \sim 300$ K) in sample chamber of 1 Pa.

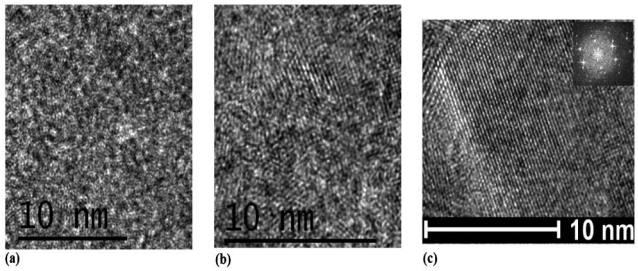

Fig. 2. TEM images exhibiting the BS structures prepared under annealing at 1000°C for (a) 2 min, (b) 8 min, or (c) 20 min, respectively, in which the figure (b) shows the crystallizing structure involving the plentiful defects related to the annealing time of 8 min.

It is noted that in the annealing effect the temperature and time are important due to the crystallizing process, in which Fig. 3(a) shows that the annealing at 1000°C is suitable for emission in the PL spectra measured in room temperature, and Fig. 3(b) indicates that the optimal annealing time is about 6 min at 1000°C for emission in the PL spectra measured at 16 K related to the defects on the BS prepared in vacuum (sample I).

It is very interesting to make a comparison between sample I prepared in vacuum and sample II prepared in oxygen with 80 Pa in the analysis of PL spectra with a change of excitation power. Figure 4(a) shows the PL spectra measured at room temperature on sample I prepared in vacuum, in which the intensity of the sharper peaks near 1600 nm super-linear increases with excitation power, and the excitation threshold is about 100 mW. In addition, the PL peaks enhanced are broader measured at room temperature on sample II prepared in oxygen with 80 Pa, as shown in Fig. 4(b), whose broader emission band relates to the plentiful impurity states in the defects of the BS. In Fig. 4(c), the super-linear increasing of the intensity occurs at the PL peaks center as shown, along with the red curve related to sample II and along with the black curve related to sample I. Here, the external quantum efficiency in the PL emission can reach to over 10% on sample II prepared in oxygen with 80 Pa in our laboratory.

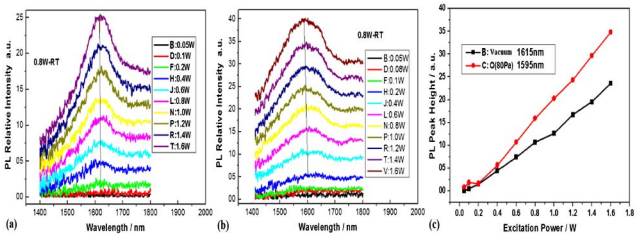

Fig. 4. Comparison of PL spectra measured at room temperatures with various excitation powers between sample I and sample II. (a) PL spectra with a change of excitation power on sample I prepared in vacuum. (b) PL spectra with a change of excitation power on sample II prepared in oxygen with 80 Pa. (c) Evolution with super-linear increasing under various excitation powers, in which the red curve relates to sample II and the black curve relates to sample I.

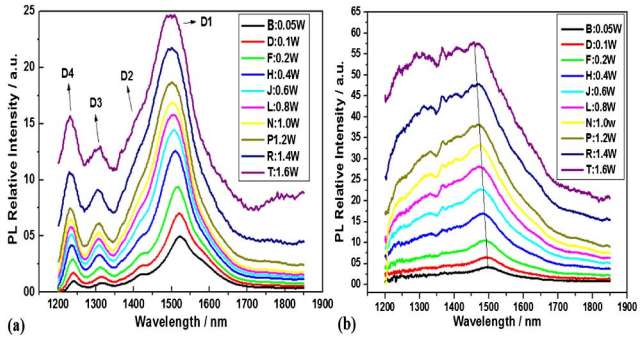

Fig. 5. PL spectra with different excitation powers measured at 16 K. (a) PL peaks under different excitation powers originated from the defects on sample I prepared in vacuum. (b) PL bands under different excitation powers related to the impurity states at the defects on sample II prepared in oxygen with 80 Pa.

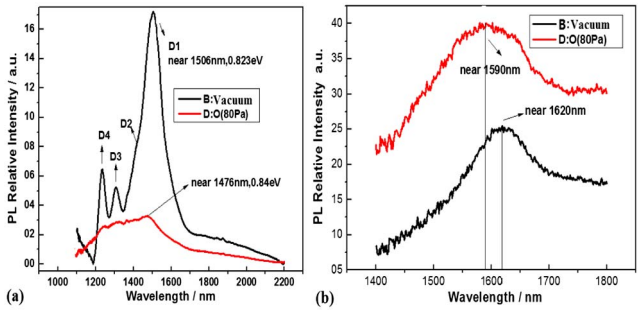

Fig. 7. Analysis of the PL spectra on samples I and II measured at different temperatures. (a) PL spectra on samples I and II measured at 16 K, in which the defects emission play a main role on sample I related to the black curve. (b) PL spectra on samples I and II measured at room temperature, in which the impurity states emission with a broader band is enhanced on sample II related to the red curve.

Figure 5 exhibits the PL spectra with different excitation powers measured at 16 K, in which the PL peaks originated from the defects D1, D2, D3, and D4 on sample I prepared in vacuum are shown in Fig. 5(a) and, on sample II, prepared in oxygen with 80 Pa the sharper PL peaks disappear taken place of the broader PL band owing to the impurity states at the defects, as shown in Fig. 5(b). The super-linear increasing of the intensity also occurs at the PL peak center measured at lower temperature.

It is interesting to make an analysis for the PL spectra at various temperature, where Fig. 6(a) shows the change of the PL peaks from the defects in different temperatures on sample I prepared in vacuum and Fig. 6(b) shows the change of the broader PL band from impurity states in different temperatures on sample II prepared in oxygen with 80 Pa.

The results of the analysis on the PL spectra demonstrate the impurity effect at the defects on the BS, in which Fig. 7(a) shows that at 16 K temperature the defects emission plays a main role related to the black curve measured on sample I but, at room temperature, the impurity states emission with a broader band related to the red curve measured on sample II is enhanced as shown in Fig. 7(b).

A physical model for the infrared emission is built on the BS, as shown in Fig. 8, in which the results of the experiment and calculation demonstrate that the defects emission related to the dislocation states D1, D2, D3, and D4 (blue lines) occurs at lower temperature and, at room temperature, the enhanced emission with a broader band relates to the impurity states (black lines) on the defects. It should be noted that the above states structure is a new distribution of the energy states in the bandgap. Here, the peaks shift in the PL spectra can be interpreted from the different position of the defect states and the impurity states on the BS.

In conclusion, we fabricate the micro-structure and nanostructure on the BS by an ns-laser. In the PL spectra on the BS structures, the enhanced emission peaks are measured in infrared wavelength for optical communication application. The annealing effect on the BS emission was observed in the analysis of the PL spectra, in which the optimal annealing temperature and the suitable annealing time have been found in the experiment, and the mechanism of the annealing effect can be interpreted from the crystallizing process on the BS. The impurity effect on the BS emission was discovered in investigation of the PL spectra at room temperature and at lower temperature, where it is interesting that impurity states localized at the defects enhance the PL emission on the BS at

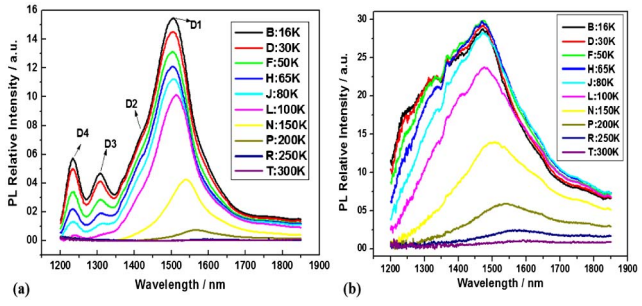

Fig. 6. PL spectra measured at various temperatures. (a) Change of the PL peaks from the defects in different temperatures on sample I prepared in vacuum. (b) Change of the broader PL bands from impurity states in different temperature on sample II prepared in oxygen with 80 Pa.

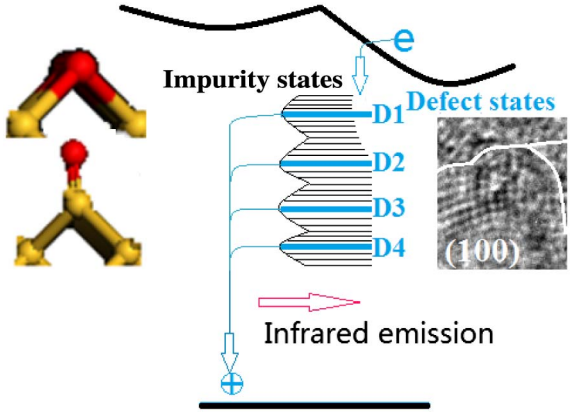

Fig. 8. Construction of a physical model for infrared emission built on the BS prepared in an oxygen environment, where it should be noted that at room temperature the enhanced emission with a broader band relates to the impurity states (black lines) on the defects which is a new distribution of the energy states.

room temperature, and the emission model involving magical states distribution in the bandgap was built to explain these effects. This is a new road to obtain emission devices for application of optical communication on a silicon chip.

Funding. National Natural Science Foundation of China (NSFC) (11264007, 61465003).

Acknowledgment. The authors thank Professor Shu-Shen Li, Professor Bao-Quan Sun, and Professor Xing-Zheng Zhang for helpful discussions and experimental measurements.

REFERENCES

1. T. H. Her, R. J. Finlay, C. Wu, S. Deliwala, and E. Mazur, Appl. Phys. Lett. **73**, 1673 (1998).
2. T. H. Her, R. J. Finlay, C. Wu, and E. Mazur, Appl. Phys. A **70**, 383 (2000).
3. M. Y. Shen, C. H. Crouch, J. E. Carey, R. Younkin, E. Mazur, M. Sheehy, and C. M. Friend, Appl. Phys. Lett. **82**, 1715 (2003).
4. H. M. Branz, V. E. Yost, S. Ward, K. M. Jones, B. To, and P. Stradins, Appl. Phys. Lett. **94**, 231121 (2009).
5. C. Wu, C. H. Crouch, L. Zhao, J. E. Carey, R. Younkin, J. A. Levinson, E. Mazur, R. M. Farrell, P. Gothoskar, and A. Karger, Appl. Phys. Lett. **78**, 1850 (2001).
6. J. E. Carey, C. H. Crouch, and E. Mazur, Opt. Photon. News **14**(2), 32 (2003).
7. J. E. Carey and E. Mazur, in *16th Annual Meeting of the IEEE Lasers and Electro-Optics Society (LEOS)* (2003), pp. 481–482
8. B. K. Nayak, V. V. Iyengar, and M. C. Gupta, Prog. Photovoltaics **19**, 631 (2011).
9. L. Pavesi, L. Dal Negro, C. Mazzoleni, G. Franzo, and E. Priolo, Nature **408**, 440 (2000).
10. W. Q. Huang, Z. M. Huang, H. Q. Chen, X. J. Miao, Q. Shu, S.-R. Liu, and C. J. Qin, Appl. Phys. Lett. **101**, 171601 (2012)
11. M. J. Smith, Y. T. Lin, M. J. Sher, M. T. Winkler, E. Mazur, and S. Gradečak, J. Appl. Phys. **110**, 053524 (2011).
12. M. Yang, Q. Wu, Z. D. Chen, B. Zhang, B. Q. Tang, J. H. Yao, D. O. Irena, and J. J. Xu, Opt. Lett. **39**, 343 (2014).
13. Q. Lü, J. Wang, C. Liang, L. Zhao, and Z. M. Jiang, Opt. Lett. **38**, 1274 (2013).
14. T. Chen, J. Si, X. Hou, S. Kanehira, K. Miura, and K. Hirao, J. Appl. Phys. **110**, 073106 (2011).
15. Z. D. Chen, Q. Wu, M. Yang, J. H. Yao, R. A. Rupp, Y. A. Cao, and J. J. Xu, Opt. Express **21**, 21329 (2013).